THE ASTROPHYSICAL JOURNAL, 464:943–953, 1996 June 20

UPDATED OPAL OPACITIES

CARLOS A. IGLESIAS AND FORREST J. ROGERS
Lawrence Livermore National Laboratory, P.O. Box 808, Livermore, CA 94550
Received 1995 October 19; accepted 1996 January 8

ABSTRACT

The reexamination of astrophysical opacities has eliminated gross discrepancies between a variety of observations and theoretical calculations; thus allowing for more detailed tests of stellar models. A number of such studies indicate that model results are sensitive to modest changes in the opacity. Consequently, it is desirable to update available opacity databases with recent improvements in physics, refinements of element abundance, and other such factors affecting the results.

Updated OPAL Rosseland mean opacities are presented. The new results have incorporated improvements in the physics and numerical procedures as well as corrections. The main opacity changes are increases of as much as 20% for Population I stars due to the explicit inclusion of 19 metals (compared to 12 metals in the earlier calculations) with the other modifications introducing opacity changes smaller than 10%. In addition, the temperature and density range covered by the updated opacity tables has been extended. As before, the tables allow accurate interpolation in density and temperature as well as hydrogen, helium, carbon, oxygen, and metal mass fractions. Although a specific metal composition is emphasized, opacity tables for different metal distributions can be made readily available. The updated opacities are compared to other work.

Subject headings: atomic data — atomic processes — stars: interiors

1. INTRODUCTION

Radiation transport plays a basic role in determining the structure and evolution of stars. Thus, as observational and modeling capabilities progress, a number of serious discrepancies become apparent that could be explained by uncertainties in the opacity. Recently, new astrophysical opacity calculations helped resolve several of these outstanding problems (e.g., Rogers & Iglesias 1994; Adelman & Wiese 1995). The most significant change was an increase of over a factor of 3 in opacity for Population I stars near temperatures of a few hundred thousand degrees due to improved atomic physics for partially ionized Fe (Iglesias, Rogers, & Wilson 1990; Iglesias & Rogers 1991a; Rogers & Iglesias 1992a; Seaton et al. 1994, hereafter SYMP). Additional improvements in the bound-bound transitions of Fe using full intermediate coupling rather than pure *LS* coupling (Iglesias, Rogers, & Wilson 1992, hereafter IRW) led to further opacity increases that affected stability studies of hot stars (Cox et al. 1992; Moskalik & Dziembowski 1992; Kiriakidis, El Eid, & Glatzel 1992; Dziembowski & Pamyatnykh 1993; Dziembowski 1994; Gautschy & Saio 1993). That is, stellar pulsation models are sensitive to $\sim 20\%$ changes in opacity. Other iron-group elements were also found to increase the opacity further by $\sim 30\%$ even though their combined abundance is more than an order magnitude smaller than that of Fe (Rogers & Iglesias 1992a; 1993; SYMP). Heavier elements (atomic number >28), however, have sufficiently low abundances in normal composition stars that their contribution to the opacity is small (Iglesias et al. 1995).

For practical reasons previously distributed OPAL opacity tables only considered 12 metals including Fe but neglecting other iron-group elements. The present work expands on the earlier calculations by including 19 metals. Additional modifications are discussed in detail below. These updated opacity tables are available for a range of mixtures with varying hydrogen and metal mass fraction. Also available are tables for C and O rich composition similar to those offered in Iglesias & Rogers (1993). These tables allow for accurate interpolation in temperature and density as well as H, He, C, O, and metal mass fraction. Although the default metal distribution assumes the solar composition from Grevesse & Noels (1993, hereafter GN93), opacity tables for different metal distributions can be readily generated on request using a correspondence between the equation of state (EOS) and opacity for sets of mixtures with the same temperature and electron density (Rogers & Iglesias 1992b).

2. MODIFICATIONS TO OPAL

The OPAL code has been previously described in detail (Rogers & Iglesias 1992a; IRW) and only subsequent modifications are discussed. These modifications have been grouped into the following three categories: physics, numerical procedures, and corrections.

2.1. *Physics*

Under this heading are included improvements to the physics as well as added cross sections. The main new feature is the consideration of seven additional metals where a sample mixture is explicitly given in Table 1. As was first shown in Rogers & Iglesias (1992a) and in more detail later by IRW and SYMP, it is important to include the spin-orbit interaction in the atomic data generation for Fe. Consequently, full intermediate coupling is used for Ar and heavier elements, while *LS* coupling is used for the lighter elements. The necessary atomic data are computed as before from parametric potentials (Rogers, Wilson, & Iglesias 1988; IRW).

In earlier OPAL tables the densities were sufficiently low and the material hot enough that the absorption by molecules was not significant and only the formation of H_2 was included in the EOS. At higher densities and lower temperatures the absorption and scattering cross sections from various H and He species can play a more important roll (Lenzuni, Chernoff, & Salpeter 1991; Stancil 1994). A list of

TABLE 1

METAL COMPOSITION

ELEMENT	RELATIVE NUMBER FRACTION: Grevesse & Noels (1993)	RELATIVE NUMBER FRACTION: Reduction[a] to 19 Metals
C	2.45518E−1	2.45518E−01
N	6.45777E−2	6.45777E−02
O	5.12959E−1	5.12966E−01
F	2.51236E−5	
Ne	8.31922E−2	8.32102E−02
Na	1.47939E−3	1.47939E−03
Mg	2.63077E−2	2.63077E−02
Al	2.04213E−3	2.04213E−03
Si	2.45518E−2	2.45518E−02
P	1.95022E−4	1.95022E−04[b]
S	1.12223E−2	1.12223E−02
Cl	2.18818E−4	2.18818E−04[b]
Ar	2.29130E−3	2.29130E−03
K	9.12184E−5	9.12184E−05[b]
Ca	1.58519E−3	1.58558E−03
Sc	1.02349E−6	
Ti	7.24574E−5	7.48770E−05[b]
V	6.91963E−6	
Cr	3.23655E−4	3.28793E−04[b]
Mn	1.69857E−4	1.69857E−04[b]
Fe	2.18818E−2	2.18771E−02
Co	5.75549E−5	
Ni	1.23050E−3	1.29276E−03[b]

[a] The reduction to 19 metals conserves molecular weight and particle number.

[b] New metals in OPAL calculation.

these cross sections new to the OPAL code is given in Table 2.

There are two modifications to the spectral line broadening. The first involves the red wings of line profiles which at low temperatures can make a significant contribution to the individual element opacity (blue wings are overwhelmed by other lines or the photoionization continuum). Unfortunately, present line-shape theories are not satisfactory in the far-wing regions. It is clear, however, that the $(\nu - \nu_0)^{-2}$ behavior of a Voigt profile in the far wing is not valid; ν is the photon frequency and ν_0 the frequency at line center. Following the proposed expedient by SYMP, the red wings of the Voigt profiles are now multiplied by the factor $(\nu/\nu_0)^4$.

The second modification to the spectral lines is broadening by neutral H and He. Typically, impact broadening by electrons overwhelms the broadening by neutrals, except at low temperatures where the electron density can be orders of magnitude smaller than the neutral particle density. At present, no simple recipe exists for accurately estimating collision broadening by neutrals. The formula for van der Waals broadening proposed by Unsöld (1955) is based on estimates of the long-range dispersion forces in terms of the hydrogen ground-state polarizability and the mean squared radius of the radiating states. This approach has been widely used but gives values that are generally too small where the corrections depend on the particular species and transitions (e.g., Gurtovenko & Kondrashova 1980).

In order to improve on the Unsöld approximation, Deridder & van Rensbergen (1976) computed the collision broadening by neutral H and He using the Smirnov-Roueff potential. In the present work, their tabulated results are used to compute the damping constants of lines from neutral and singly charged metals broadened by neutral H and He.

In IRW and earlier OPAL calculations the ionization balance was computed in the Debye-Hückle approximation. This approach is valid over most of the density-temperature range covered by the tables since these plasmas are weakly coupled (i.e., kinetic energy $\gg$ potential energy). At the higher densities, however, the Debye-Hückle approximation is no longer valid and the occupation of weakly bound states in highly ionized ions is sensitive to higher order Coulomb corrections (e.g., see Fig. 1 of Iglesias & Rogers 1993). Consequently, the present calculations include these higher order Coulomb terms (Rogers, Swenson, & Iglesias 1996).

TABLE 2

NEW ABSORPTION AND SCATTERING CROSS SECTIONS

Reaction	Reference
Induced collision absorption by H_2	Lenzuni et al. 1991
H_2 Rayleigh scattering	Dalgarno & Williams 1966
$H_2 + e^- + h\nu \rightarrow H + H^+$	Bell 1980
$H + H^+ + h\nu \rightarrow H + H^+$	Stancil 1994
$H_2^+ + h\nu \rightarrow H^+ + H$	Stancil 1994
$H_2^+ + e^- + h\nu \rightarrow H_2^+ + e^-$	$\sigma(p + e^- + h\nu \rightarrow p + e^-)$[a]
$He + He^+ + h\nu \rightarrow He + He^+$	Stancil 1994
$He_2^+ + h\nu \rightarrow He^+ + He$	Stancil 1994
$He_2^+ + e^- + h\nu \rightarrow He_2^+ + e^-$	$\sigma(p + e^- + h\nu \rightarrow p + e^-)$[a]

[a] This process is assumed equal the proton and electron inverse bremsstrahlung cross section.

2.2. *Numerical Procedures*

Although the temperature resolution in previous OPAL tables was considered adequate for interpolation (Rogers & Iglesias 1992a; Seaton 1993), stellar pulsation models are sensitive to temperature derivatives of the opacity. Therefore, the number of temperature points has been increased; in particular, for the important region between 10^5 and 10^6 K where the opacities display large increases relative to the Los Alamos results (e.g., Huebner et al. 1977). A sample Rosseland mean opacity table is given in Table 3 to be compared to previous tabulations (e.g., Table 2 of IRW). The tables are in terms of $\log R = \log(\rho/T_6^3)$ and $\log T$, where ρ is the mass density in g cm^{-3}, $T_6 = 10^{-6}\,T$, and T is the temperature in kelvins. The range of the tables has been extended in both temperature and density; the new ranges are $3.75 \leq \log T \leq 8.7$ and $-8 \leq \log R \leq +1$. The lowest temperature is sufficiently high that the neglect of molecular absorption (except for those in Table 2) should not lead to significant errors (Alexander & Ferguson 1994). Also note that the tables are almost rectangular except for missing entries at the highest densities and temperatures. The omitted values correspond to degenerate plasmas that are beyond the range of validity of the calculations but where the energy transport is dominated by conduction (Cox & Giuli 1968). The cutoff roughly corresponds to a degeneracy parameter $\eta = (\text{chemical potential}/k_B T) = 8$, where k_B is the Boltzmann constant.

The number of frequency points in the monochromatic photoabsorption has doubled to 10^4, still covering the same energy range 0–$20k_B T$. Even though it was found earlier (Rogers & Iglesias 1992a) that 5000 points was reasonably accurate for Rosseland mean opacity calculations (largest errors were a few percent) and that increasing the number of frequency points only marginally reduces the uncertainties, using 10^4 points assures that the photon energy mesh is not responsible for differences with other calculations.

TABLE 3

SAMPLE ROSSELAND MEAN OPACITY TABLE FOR $X = 0.7$ AND $Z = 0.02$ WITH METAL DISTRIBUTION FROM GN 93[a]

log$T$	log R=																		
	-8.0	-7.5	-7.0	-6.5	-6.0	-5.5	-5.0	-4.5	-4.0	-3.5	-3.0	-2.5	-2.0	-1.5	-1.0	-0.5	0.0	0.5	1.0
3.75	-0.767	-0.928	-1.119	-1.327	-1.542	-1.754	-1.955	-2.126	-2.236	-2.251	-2.166	-2.007	-1.799	-1.573	-1.304	-0.991	-0.645	-0.261	0.131
3.80	-0.561	-0.598	-0.675	-0.794	-0.944	-1.109	-1.273	-1.408	-1.493	-1.500	-1.425	-1.293	-1.107	-0.916	-0.688	-0.442	-0.180	0.121	0.429
3.85	-0.534	-0.530	-0.525	-0.525	-0.543	-0.588	-0.649	-0.706	-0.739	-0.725	-0.663	-0.552	-0.406	-0.247	-0.051	0.161	0.384	0.628	0.894
3.90	-0.536	-0.526	-0.508	-0.472	-0.407	-0.314	-0.212	-0.120	-0.042	0.027	0.102	0.194	0.310	0.431	0.589	0.765	0.954	1.158	1.377
3.95	-0.537	-0.529	-0.512	-0.475	-0.396	-0.256	-0.046	0.205	0.446	0.640	0.781	0.894	0.997	1.098	1.220	1.359	1.511	1.684	1.877
4.00	-0.518	-0.521	-0.513	-0.483	-0.411	-0.267	-0.034	0.287	0.651	0.994	1.262	1.450	1.587	1.699	1.806	1.913	2.040	2.184	2.348
4.05	-0.490	-0.489	-0.486	-0.469	-0.413	-0.283	-0.052	0.280	0.683	1.111	1.500	1.809	2.030	2.184	2.302	2.410	2.518	2.639	2.774
4.10	-0.479	-0.474	-0.464	-0.444	-0.395	-0.286	-0.083	0.226	0.626	1.075	1.529	1.945	2.274	2.515	2.687	2.819	2.936	3.050	3.172
4.15	-0.469	-0.458	-0.445	-0.424	-0.376	-0.273	-0.089	0.186	0.553	0.990	1.467	1.941	2.365	2.707	2.954	3.132	3.275	3.400	3.521
4.20	-0.473	-0.458	-0.437	-0.409	-0.361	-0.265	-0.093	0.168	0.512	0.924	1.387	1.882	2.359	2.787	3.131	3.380	3.560	3.709	3.841
4.25	-0.474	-0.460	-0.439	-0.407	-0.353	-0.256	-0.096	0.147	0.479	0.882	1.337	1.818	2.315	2.798	3.223	3.552	3.794	3.983	4.141
4.30	-0.465	-0.453	-0.434	-0.404	-0.354	-0.262	-0.103	0.132	0.452	0.853	1.313	1.798	2.293	2.798	3.271	3.675	3.983	4.222	4.409
4.35	-0.452	-0.441	-0.421	-0.390	-0.340	-0.255	-0.110	0.121	0.445	0.854	1.316	1.807	2.313	2.817	3.316	3.771	4.141	4.433	4.652
4.40	-0.430	-0.421	-0.403	-0.369	-0.314	-0.231	-0.098	0.116	0.437	0.849	1.317	1.822	2.346	2.864	3.381	3.863	4.278	4.612	4.861
4.45	-0.420	-0.406	-0.383	-0.344	-0.280	-0.185	-0.047	0.164	0.477	0.889	1.362	1.871	2.399	2.929	3.462	3.963	4.406	4.764	5.048
4.50	-0.415	-0.403	-0.380	-0.336	-0.258	-0.142	0.013	0.225	0.529	0.931	1.404	1.920	2.456	3.003	3.548	4.063	4.524	4.903	5.202
4.55	-0.408	-0.393	-0.371	-0.332	-0.254	-0.120	0.070	0.316	0.634	1.027	1.488	1.998	2.528	3.077	3.627	4.152	4.620	5.008	5.313
4.60	-0.413	-0.397	-0.372	-0.332	-0.255	-0.119	0.093	0.386	0.740	1.142	1.593	2.083	2.599	3.138	3.687	4.213	4.680	5.067	5.365
4.65	-0.411	-0.397	-0.376	-0.338	-0.264	-0.129	0.088	0.399	0.797	1.239	1.699	2.177	2.672	3.190	3.721	4.231	4.687	5.065	5.353
4.70	-0.410	-0.395	-0.375	-0.341	-0.277	-0.152	0.059	0.367	0.766	1.229	1.721	2.217	2.709	3.208	3.715	4.202	4.640	5.008	5.288
4.75	-0.410	-0.393	-0.370	-0.340	-0.281	-0.169	0.028	0.325	0.712	1.167	1.664	2.180	2.688	3.186	3.674	4.139	4.561	4.919	5.203
4.80	-0.409	-0.392	-0.371	-0.339	-0.282	-0.178	0.005	0.284	0.654	1.094	1.579	2.094	2.618	3.129	3.613	4.066	4.477	4.828	5.107
4.85	-0.411	-0.395	-0.372	-0.339	-0.285	-0.186	-0.012	0.256	0.609	1.031	1.505	2.011	2.537	3.056	3.547	4.000	4.407	4.751	5.019
4.90	-0.402	-0.388	-0.368	-0.335	-0.279	-0.183	-0.019	0.235	0.577	0.985	1.447	1.950	2.473	2.994	3.493	3.951	4.357	4.691	4.941
4.95	-0.381	-0.367	-0.347	-0.318	-0.266	-0.173	-0.014	0.232	0.567	0.969	1.422	1.916	2.433	2.953	3.455	3.918	4.321	4.642	4.867
5.00	-0.339	-0.331	-0.315	-0.288	-0.239	-0.153	-0.004	0.234	0.565	0.968	1.416	1.902	2.416	2.930	3.434	3.896	4.290	4.591	4.788
5.05	-0.269	-0.258	-0.245	-0.223	-0.181	-0.102	0.039	0.266	0.590	0.987	1.429	1.915	2.420	2.921	3.418	3.870	4.246	4.521	4.693
5.10	-0.198	-0.180	-0.160	-0.132	-0.091	-0.019	0.109	0.313	0.607	0.990	1.437	1.916	2.412	2.916	3.395	3.823	4.171	4.422	4.579
5.15	-0.157	-0.120	-0.083	-0.040	0.015	0.097	0.221	0.407	0.678	1.038	1.467	1.935	2.419	2.904	3.353	3.744	4.061	4.293	4.447
5.20	-0.163	-0.113	-0.058	0.006	0.085	0.188	0.330	0.522	0.776	1.105	1.509	1.960	2.423	2.878	3.286	3.633	3.921	4.144	4.308
5.25	-0.215	-0.157	-0.089	-0.008	0.091	0.219	0.385	0.591	0.841	1.149	1.531	1.962	2.405	2.829	3.195	3.503	3.768	3.987	4.166
5.30	-0.281	-0.220	-0.147	-0.060	0.051	0.196	0.381	0.607	0.872	1.180	1.539	1.945	2.365	2.758	3.088	3.365	3.613	3.832	4.025
5.35	-0.357	-0.305	-0.236	-0.147	-0.035	0.113	0.310	0.555	0.842	1.161	1.517	1.904	2.302	2.671	2.973	3.228	3.465	3.685	3.887
5.40	-0.410	-0.372	-0.317	-0.240	-0.137	0.003	0.197	0.456	0.767	1.110	1.472	1.848	2.230	2.577	2.858	3.097	3.326	3.548	3.754
5.45	-0.444	-0.421	-0.381	-0.319	-0.226	-0.093	0.094	0.354	0.681	1.043	1.416	1.788	2.155	2.483	2.747	2.974	3.199	3.422	3.626
5.50	-0.457	-0.446	-0.423	-0.380	-0.306	-0.189	-0.014	0.239	0.571	0.955	1.349	1.729	2.083	2.394	2.643	2.861	3.083	3.307	3.508

TABLE 3—*Continued*

log$T$	log R=																		
	-8 0	-7.5	-7 0	-6 5	-6 0	-5 5	-5 0	-4 5	-4 0	-3 5	-3 0	-2.5	-2 0	-1 5	-1 0	-0 5	0 0	0 5	1 0
5 55	-0 463	-0 457	-0.446	-0 420	-0 368	-0 272	-0 112	0 136	0 479	0 881	1 290	1 669	2.014	2 310	2 548	2 759	2 979	3 202	3 399
5 60	-0 465	-0 462	-0 455	-0 440	-0.407	-0 338	-0 199	0 039	0 387	0 807	1 230	1 614	1.952	2.235	2 463	2 669	2 887	3 108	3 304
5 65	-0 466	-0 463	-0 458	-0 448	-0 428	-0 383	-0 280	-0 070	0 272	0 711	1 159	1.557	1.894	2 167	2 388	2 592	2 804	3 021	3 226
5 70	-0 467	-0.464	-0.459	-0 451	-0.436	-0 403	-0 327	-0 158	0 160	0 604	1.078	1 498	1.837	2 108	2 325	2 527	2 735	2 947	3 167
5 75	-0 467	-0 465	-0.460	-0 453	-0 440	-0 413	-0 355	-0.223	0 053	0 490	0 986	1 429	1 780	2 051	2 269	2 470	2 671	2.877	3 103
5 80	-0 467	-0.465	-0 461	-0.454	-0.441	-0 417	-0 367	-0 258	-0 027	0 378	0 882	1 348	1 715	1 994	2.216	2 418	2 616	2 818	3.041
5 85	-0 467	-0 465	-0 462	-0 455	-0 443	-0 419	-0 374	-0 278	-0 074	0 293	0 783	1 263	1 647	1 935	2 165	2 369	2 566	2 770	2 998
5.90	-0 467	-0 465	-0 462	-0.457	-0 445	-0 423	-0 379	-0.290	-0 108	0.223	0 691	1.178	1.577	1 877	2 116	2.325	2 522	2 724	2.947
5 95	-0 466	-0.464	-0 460	-0 455	-0 444	-0.423	-0 382	-0 298	-0 128	0 180	0.623	1.103	1 512	1.825	2 073	2.287	2.481	2 676	2 886
6 00	-0.464	-0.461	-0 457	-0 451	-0 441	-0 422	-0 383	-0 302	-0 137	0 159	0 585	1 054	1 464	1 784	2 039	2.255	2 441	2 625	2 840
6 10	-0.466	-0 460	-0 452	-0 442	-0 429	-0.409	-0 374	-0.303	-0 152	0 118	0 507	0.956	1 373	1.712	1 980	2 187	2 353	2 530	2 738
6 20	-0 471	-0.468	-0.462	-0 450	-0.429	-0 397	-0.352	-0 280	-0 146	0 092	0 449	0 882	1 301	1 643	1 898	2 080	2 217	2 387	2.621
6 30	-0 472	-0 471	-0 469	-0 465	-0 453	-0 424	-0.365	-0 268	-0 120	0 104	0 432	0 838	1 230	1 544	1.765	1 915	2 054	2 240	2 489
6 40	-0.473	-0 472	-0 471	-0.470	-0 465	-0 451	-0 415	-0 323	-0.146	0 109	0.431	0.796	1 127	1 383	1 573	1 718	1.874	2 089	2 353
6 50	-0 474	-0 473	-0 473	-0 472	-0 469	-0.462	-0 441	-0 382	-0.236	0 029	0.367	0 695	0.968	1 179	1 354	1 513	1 701	1 941	2 208
6 60	-0.474	-0 474	-0 474	-0.473	-0 471	-0 467	-0 453	-0.414	-0.312	-0.099	0 213	0 522	0 768	0.962	1 135	1 316	1.536	1 799	2.074
6.70	-0.476	-0.475	-0 475	-0 475	-0 474	-0.470	-0 461	-0 433	-0 362	-0 205	0 048	0.325	0 558	0.750	0 931	1 133	1 382	1.660	1 938
6 80	-0 477	-0.477	-0 477	-0 476	-0 476	-0 473	-0 467	-0 448	-0 398	-0 283	-0.090	0 141	0 357	0.552	0 747	0.974	1 247	1 535	1.792
6.90	-0.478	-0.478	-0 478	-0 478	-0 477	-0.475	-0 470	-0 457	-0 421	-0 340	-0 195	-0 004	0 193	0 387	0.601	0.845	1 127	1.410	1 647
7 00	-0 480	-0.480	-0 480	-0.480	-0 479	-0 476	-0 471	-0 460	-0 433	-0 373	-0 266	-0 115	0 066	0.270	0 493	0 742	1 020	1 285	1 513
7.10	-0 483	-0 483	-0 483	-0 482	-0.482	-0 480	-0 474	-0 460	-0 433	-0 382	-0 297	-0 171	-0.003	0 190	0 400	0 638	0 909	1 161	1 336
7.20	-0.486	-0 486	-0.486	-0 486	-0.485	-0.484	-0 480	-0 467	-0.438	-0.386	-0 308	-0 195	-0 050	0 116	0 302	0.533	0 787	1 027	
7 30	-0.490	-0.490	-0 490	-0.490	-0 490	-0.489	-0 486	-0 477	-0 454	-0 406	-0 329	-0.224	-0.105	0 030	0 199	0 420	0.681		
7 40	-0 495	-0 495	-0 495	-0 495	-0 495	-0 494	-0 492	-0.487	-0 471	-0 434	-0 367	-0 276	-0.177	-0 061	0 102	0 319	0 567		
7.50	-0.501	-0.501	-0.501	-0 501	-0 501	-0 501	0 499	-0 495	-0 485	-0 460	-0 409	-0.336	-0 251	-0.144	0 010	0 226			
7 60	-0.508	-0 508	-0.508	-0 508	-0.509	-0 509	-0 508	-0 505	-0 498	-0 481	-0 444	-0.387	-0 315	-0.217	-0 073	0.127			
7 70	-0 518	-0 518	-0 518	-0 518	-0.518	-0.518	-0 517	-0 516	-0 511	-0 498	-0.471	-0.429	-0.370	-0 283	-0 153	0 026			
7 80	-0.530	-0 530	-0.530	-0 530	-0 530	-0 530	-0.529	-0 529	-0.525	-0 515	-0.495	-0 463	-0 418	-0.346	-0.234	-0 088			
7.90	-0 544	-0 544	-0 544	-0 544	-0 545	-0 545	-0 544	-0.544	-0.541	-0 533	-0 519	-0 497	-0 465	-0 411	-0 318				
8 00	-0 560	-0 560	-0 560	-0.560	-0.560	-0.561	-0.561	-0.560	-0.558	-0 552	-0 542	-0 530	-0.512	-0 475	-0 403				
8 10	-0.580	-0.580	-0.580	-0 580	-0 580	-0.580	-0.581	-0.581	-0 578	-0 574	-0 569	-0 566	-0 562	-0.544	-0 500				
8 30	-0 633	-0 633	-0 633	-0 633	-0 634	-0 634	-0 634	-0 633	-0.633	-0.633	-0 638	-0.654	-0 678	-0 698	-0.716				
8 50	-0.704	-0 704	-0 704	-0 704	-0.704	-0.704	-0 704	-0.704	-0 705	-0 710	-0.724	-0 759	-0.798	-0.915	-1 269				
8 70	-0.582	-0.753	-0 785	-0 789	-0.789	-0 789	-0 789	-0 789	-0.792	-0.801	-0.826	-0 882	-0 941	-1.081					

[a] Values of log κ_R are presented with κ_R in cm^2 g^{-1}

Although there are no computational restrictions on the total number of transition arrays or spectral lines for a given ion stage, there is a maximum number of spectral lines allowed within a transition array connecting two configurations. Originally this number was set at 10^4 for the *LS* coupling calculations (Rogers & Iglesias 1992a) and was later increased to 5×10^4 for the full intermediate coupling results (IRW). It has been increased again to 1.5×10^5. As a result, almost all transition arrays considered could be treated in full detail except for a few weak transition arrays in Fe and Ni which were treated in pure *LS* coupling.

2.3. *Corrections*

The development of the OPAL code has continued up to the present and in the process some errors have been found. Fortunately, only a couple of these errors have significantly affected the astrophysical opacities. One such correction was a factor of 2 overestimate in the natural line widths. A second involves the table generation code that combines the individual element monochromatic opacities and leads to errors at the lowest temperature. There have been other minor corrections. For example, a systematic error of $\sim 15\%$ in some $2s$–$2p$ transitions for initial electron configuration $1s^2 2s^2 2p^x nl$ with $1 \leq x \leq 5$ was reduced to a few percent or less. This $\sim 15\%$ error in a few spectral lines is large when comparing to spectroscopic measurements, but it had negligible effect on the Rosseland mean opacities of astrophysical mixtures.

3. RESULTS

The main opacity changes are due to the additional metals in the mixture. Their impact as well as those from the other modifications in § 2 are considered in more detail below. Before proceeding, note that the improvements in the numerical procedures (§ 2.2) have little effect on the astrophysical opacities. The larger number of lines in a given transition array did increase the Rosseland mean opacity of the heaviest elements when considered individually at conditions relevant to stellar envelopes. Nevertheless, once the elements are combined to make a typical stellar composition the differences vanish from the final results. As mentioned above, increasing the number of photon energy points had negligible impact on the Rosseland mean opacity. One possible exception is the increased temperature resolution of the tables which could affect opacity derivatives.

The various improvements and corrections influenced different regions of the opacity tables. Generally, the modifications led to moderate net increases in the opacity, but there is an important region in the tables where the opacities are now smaller. For an overview, the ratios of opacities from the present work to the IRW results are displayed in Figure 1. The comparisons are for mixtures with hydrogen mass fraction $X = 0.7$ and metal mass fraction $Z = 0.02$ and 0.001 where the metal composition is given in Table 1. Throughout the discussion the helium mass fraction, Y, is adjusted so that $X + Y + Z = 1$. Note that in reducing the mixture in Table 1 from 19 to 12 metals for the IRW calculations, the particle number as well as the molecular weight of the mixture is conserved. For example, the Fe abundance in the 14 element composition is slightly larger than in the 21 element mixture to compensate for the missing iron-group elements. In Figure 1*a* the $\log R = -5.5$ track is representative of plasma conditions relevant to stability studies of hot stars for which the 20% opacity enhancement near $\log T = 5.3$ is significant, $\log R = -3.5$ is representative of envelopes in Population I Classical Cepheids, and $\log R = -1.5$ shows a 5% decrease in opacity near $\log T = 6.3$ that is relevant to solar interior models. Because of the lower metallicity, Figure 1*b* shows much reduced opacity changes.

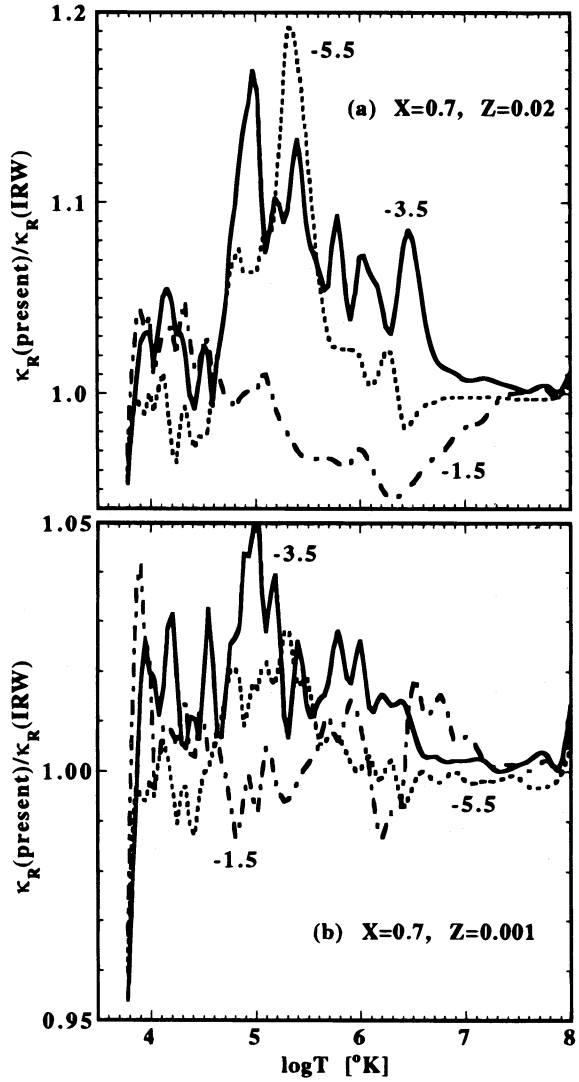

FIG. 1.—Ratio of updated OPAL and IRW Rosseland mean opacities as a function of temperature at constant log R values indicated in the Figure. The plots are for $X = 0.7$ and (*a*) $Z = 0.02$ plus (*b*) $Z = 0.001$ where the metal distribution is from Table 1.

3.1. *Effect of Additional Metals*

Although the seven additional elements constitute less than 0.25% of the total metal abundance in Table 1, their impact on the opacity is not negligible. In Figure 2 the ratio of the opacity computed with the updated OPAL code with 21 and 14 elements is plotted where the latter composition consists of those element explicitly included in IRW. Again, when reducing the mixture in Table 1 from 19 to 12 metals, the particle number as well as the molecular weight of the mixture is conserved. The $\log R = -5.5$ track in Figures 1*a* and 2*a* is not only representative of pulsating hot stars, but also of the largest opacity enhancements.

Not surprisingly, the ratios for $Z = 0.02$ and 0.001 in Figure 2 have similar shape except that the opacity

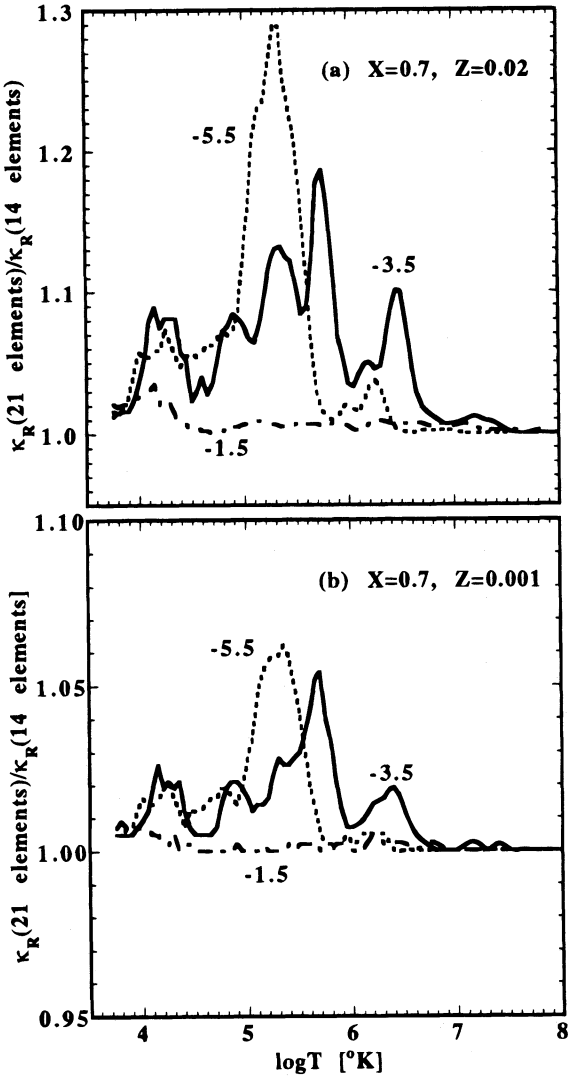

FIG. 2.—Ratio of Rosseland mean opacities computed with 21 and 14 elements for the same mixtures as in Fig. 1 at constant log R values indicated in the figure.

enhancements are smaller for the lower metallicity mixture. A comparison of Figures 1 and 2 shows that the main modification to the IRW opacities is the explicit presence of the seven additional metals. Note that their effect at log $R = -3.5$ is evident even at the higher temperatures.

Not all of the seven additional metals in Table 1 contribute equally to the opacity. By far the largest opacity enhancements are due to Ni which is both the heaviest and most abundant of the additional elements. On the other hand, less than 1% change in opacity is produced by individually adding P, Cl, or K to a mixture with $X = 0.7$ and $Z = 0.02$. For the same composition each of the remaining three metals (Ti, Cr, and Mn) contributes at the few percent level with Cr producing close to a 10% opacity increase at log $R = -5.5$ and log $T = 5.1$.

3.2. *Line Broadening*

The effect of broadening by neutral H and He is shown in Figure 3 where the ratio of the opacity for a Population I composition with and without this broadening mechanism is presented. The figure shows that the effect is quite pronounced for Fe but not as much for the total mixture.

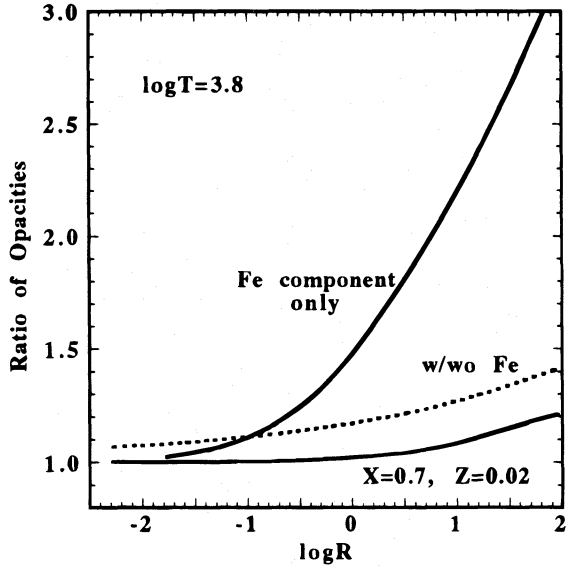

FIG. 3.—Ratio of Rosseland mean opacities computed with and without line broadening by neutral H and He as a function of R at constant temperature. The plots are for a $X = 0.7$ and $Z = 0.02$ mixture as well as the Fe component in that mixture. Also plotted is the ratio of the opacity with and without the Fe photoabsorption (*dashed line*) for the same mixture including the broadening by neutral H and He.

Similar opacity enhancements have been obtained by the Opacity Project (OP) using observationally determined widths for the Fe lines (Seaton 1994, private communication). In order to ascertain the relevant importance of Fe at these plasma conditions, the figure also displays the ratio of the opacity computed with and without the Fe photoabsorption contribution (i.e., the Fe is included in the EOS only). Clearly, the Fe photoabsorption makes a significant contribution to the opacity, and the broadening by neutral H and He of the Fe lines is important at the higher densities. Although not emphasized in Figure 3, neutral broadening by H and He is also included in spectral lines from all neutral and singly ionized metals.

The correction to the natural width does lower the mixture opacity in low density regions where pressure broadening does not dominate the line shape. This correction, which can lower the mixture opacity by as much as 10%, is most pronounced at lower R values and accounts for the reduced enhancement at log $R = -5.5$ in Figure 2*a* relative to that in Figure 1*a*. This correction partially explains the differences in Figure 15 of SYMP for the lower log R tracks and $5 \leq \log T \leq 6$. The $(v/v_0)^4$ cutoff in the red wings can significantly decrease the individual element opacities at low temperatures as shown by SYMP. It has, however, negligible impact on the opacities of hydrogen-helium–rich mixtures.

3.3. H *and* He *Cross Sections*

In the range of plasma conditions covered here the contribution from collision-induced photoabsorption by H_2 remains small (e.g., Lenzuni et al. 1991). For example, a mixture with $X = 0.7$, $Z = 0.02$, log $T = 3.75$, and log $R = +1$ has less than 1% of the hydrogen in molecular H_2. The other cross sections involving H, H^+, and H_2^+ in Table 2 do affect the opacity as shown in Figure 4. Note that these cross sections from Stancil (1994) stop at 25,200 K corresponding to the high-temperature cutoff in the figure. The

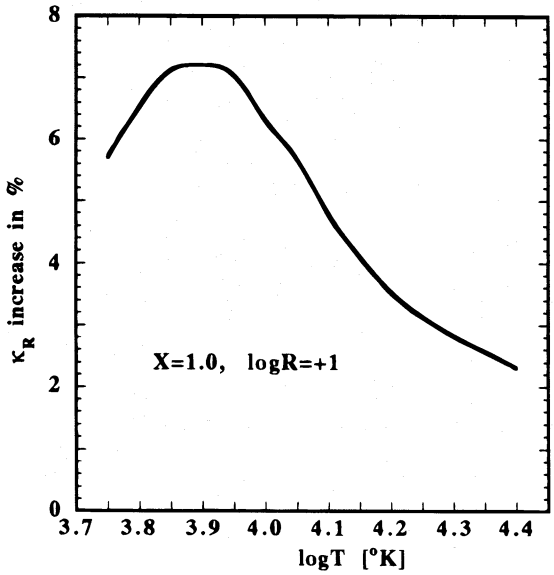

FIG. 4.—Rosseland mean opacity increases due to the cross sections in Table 2 for a pure hydrogen plasma.

comparable cross sections for the He species do not significantly contribute to the opacity for conditions considered in the present work.

3.4. *Solar Opacities*

The largest uncertainties in solar interior opacities are due to EOS models and element composition (Iglesias & Rogers 1991b, 1995; Rozsnyai 1992; Luo 1994). Consequently, the updated opacities for solar models are expected to differ from the IRW results. The ratio of updated results for 21 elements, GN93 metal composition to the IRW opacities computed with 14 elements, and the Grevesse (1991, hereafter G91) metal composition are displayed in Figure 5 for conditions relevant to the solar interior. This ratio has a minimum at log $T \approx 6.2$ (near the bottom of the solar convection zone). To isolate the improved EOS effects on the opacity, Figure 5 compares results from the present calculations and the IRW results for an identical 14 element composition and GN93 metal distribution. These opacity differences tend to vanish with decreasing temperature since $\rho \sim T^3$, thus reducing the plasma coupling and the effects of the higher order Coulomb terms. At the higher temperatures the ratio also approaches unity, since bound states are rare and do not contribute to the opacity. A third comparison emphasizes opacity changes due to changes in composition. Figure 5 shows the ratio of updated opacities computed with 21 elements for the GN93 and G91 metal compositions. In Figure 5 the improved EOS and mixture effects tend to cancel except near log $T = 6.2$ where the decrease from the modifications to the EOS are largest and increases from the new composition smallest.

3.5. *Inverse Bremsstrahlung*

At high temperatures relativistic effects can modify opacity calculations. An important contribution at these conditions is photon scattering for which OPAL includes collective effects (Boercker 1987) and relativistic corrections (Sampson 1959). For example, in Table 3 at log $T = 8.7$ and log $R = -8$ the opacity is enhanced by the relative increase of the electron-positron pair concentration. On the other hand, the inverse bremsstrahlung calculation includes collective effects but neglects relativistic corrections. Using the Bethe-Heitler results (Heitler 1954) for the Coulomb potential, it has been shown by Itoh, Masayuki, & Kohyama (1985) and by Itoh, Kojo, & Masayuki (1990) that relativistic corrections can be important in inverse bremsstrahlung calculations at conditions relevant to stellar models. Nevertheless, the relativistic corrections to the inverse bremsstrahlung only affect the total Rosseland mean opacity in the high-temperature, degenerate region of the updated tables. Note that relativistic effects also enhance the inverse bremsstrahlung cross section at high temperatures and low densities, but there the opacity is dominated by photon scattering.

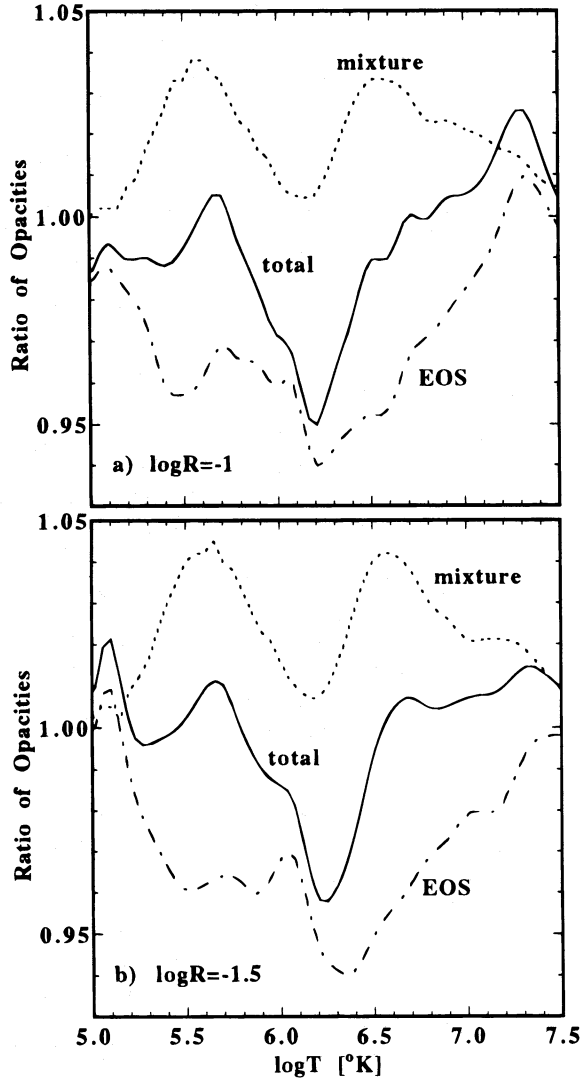

FIG. 5.—Ratio of Rosseland mean opacities for a solar mixture with $X = 0.708$, and $Z = 0.0173$ at (*a*) log $R = -1$ and (*b*) log $R = -1.5$. The ratios compare net changes in the updated opacity from IRW (*solid line*), improved EOS (*dot-dashed line*), and GN93 vs. G91 composition (*dashed line*).

Table 4 compares the total Rosseland mean opacity of a pure oxygen plasma where the inverse bremsstrahlung has been computed in the Born-Elwert approximation (Elwert 1939) for (1) nonrelativistic Coulomb potential, (2) relativistic Coulomb potential, and (3) nonrelativistic screened Coulomb potential. The last approximation uses an exponential screening length obtained from the many-body analysis (Rogers 1981) but neglects dynamic effects as well

TABLE 4

IMPACT OF INVERSE BREMSSTRAHLUNG APPROXIMATIONS[a] ON κ_R FOR A PURE OXYGEN PLASMA

	log R			
log T	−2.5	−2.0	−1.5	−1.0
8.0.....	<1%[b], <1%[c]	2%, <1%	7%, 1%	21%, 3%
8.1.....	<1%, <1%	2%, 1%	8%, 2%	26%, 5%
8.3.....	1%, 1%	4%, 3%	6%, 7%	40%, 17%
8.5.....	1%, 2%	5%, 7%	20%, 20%	62%, 350%
8.7.....	2%, 6%	9%, 17%	28%, 51%	

[a] Changes to total Rosseland mean opacity rounded off to nearest 1%.
[b] Percent *decrease* due to screening of Coulomb potential.
[c] Percent *increase* due to relativistic corrections.

as ion correlations (e.g., Ichimaru 1973). The required thermal average in all three calculations includes degeneracy effects (e.g., Itoh et al. 1985). The comparisons in Table 4 are between approximations (3) and (1) plus approximations (2) and (1). Since screening effects are important over a larger region of the opacity tables and there is no simple expression for the screened Coulomb potential (e.g., see Koch & Motz 1959), relativistic corrections are neglected in the inverse bremsstrahlung calculations and approximation (3) is used to generate the opacity tables. Consequently, Table 4 identifies an uncertain region in these tables. Fortunately, at these conditions electron conduction should dominate the energy transport.

In addition, there are contributions from electron-electron and electron-positron bremsstrahlung that are neglected in the present calculations. These contributions to the Rosseland mean opacity tables, however, are expected to be small. Even though the electron-positron cross section can be larger than the electron-ion result (Huang 1987), the pair concentration is negligible except at the highest temperature and lowest density point where the opacity is dominated by photon scattering. The ratio of the electron-electron to the electron-ion bremsstrahlung cross section can be estimated by (Maxon 1972)

$$\frac{\sigma_{ee}}{Z_i \sigma_{ei}} \approx \left[0.85 + 1.35\sqrt{\frac{h\nu}{k_B T}} + 0.38\left(\frac{h\nu}{k_B T}\right)\right]\left(\frac{k_B T}{mc^2}\right), \quad (1)$$

where mc^2 is the electron rest mass energy. This rate equals 0.21 for photon energy $h\nu/k_B T = 4$ (peak of the Rosseland function), ion charge $Z_i = 2$ (helium), and log $T = 8.7$ (maximum T in the tables). Nevertheless, the electron-electron contribution decreases linearly with T and the total contribution from inverse bremsstrahlung at high temperatures decreases with density. Consequently, only the high T and large R region of the tables are affected, but this region is already uncertain (see Table 4) and the energy transport is dominated by conduction of degenerate electrons. In order to account for electron-electron inverse bremsstrahlung it is tempting to modify the electron-ion cross section by the factor in equation (1). In the region where this contribution is most important to the total opacity, however, both plasma screening and degeneracy effects are also important and these have been neglected in obtaining equation (1).

4. COMPARISONS WITH OTHER CALCULATIONS

4.1. *Comparison to Los Alamos*

Previous work (e.g., Iglesias & Rogers 1991b, 1993; Rogers & Iglesias 1992a) made extensive comparisons to the Los Alamos opacities and discussed the source of the discrepancies. The modifications in the present work do not significantly alter those comparisons. The exception is for conditions relevant to the solar interior where models are sensitive to small changes in opacity. Consequently, it is interesting to revisit the work for the solar radiative interior (Iglesias & Rogers 1991b). These earlier comparisons were done for the Grevesse (1984) solar abundance and are reproduced in Figure 6. In addition, the results from the present calculations using the same Grevesse (1984) mixture are presented. The improved agreement in Figure 6 between the updated OPAL and Los Alamos opacities is due to the higher order Coulomb corrections in the OPAL EOS and is probably fortuitous, since plasma effects in the Los Alamos work are included through an ad hoc continuum lowering model (Huebner 1986).

4.2. *Comparison to* OP

Comparisons showing reasonably good agreement between OPAL and OP opacities for a variety of compositions have been previously discussed by SYMP. Therefore, the comparisons here are limited to those in Figures 7 and 8 plus those in Figures 11 and 12 in the next subsection. In Figures 7 and 8 the calculations are for a composition with $X = 0.7$, $Z = 0.02$, and metal distribution from SYMP, except that the OPAL and OP results include 21 and 17 elements, respectively.

Figure 7 can be compared to Figure 18 of SYMP, which again shows that the main change in the updated OPAL opacities are in the region near log $T = 5.3$. In order to emphasize the discrepancies, ratios of OPAL to OP opacities are plotted in Figure 8. Clearly, both calculations predict comparable Z-bumps near log $T = 5.3$ except for a relative shift in temperature. This, of course, is the region of the Z-bump absent in the Los Alamos opacities (e.g., Huebner et al. 1977) that has led to the resolution of several long-standing problems (e.g., Rogers & Iglesias 1994; Adelman & Wiese 1995). The Z-bump was theoretically predicted by the improved treatment of bound-bound tran-

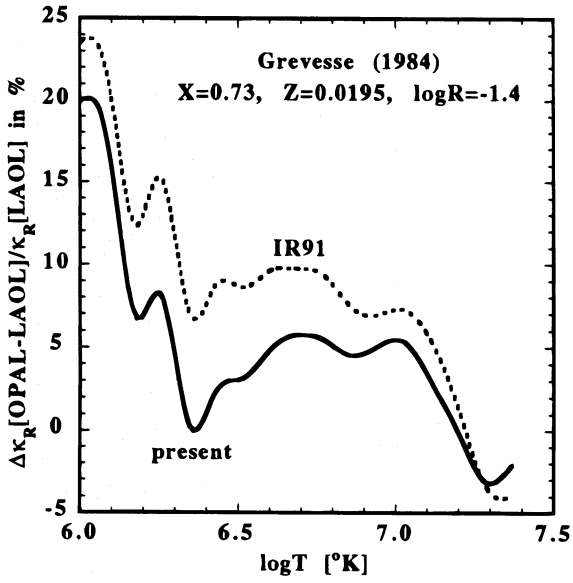

FIG. 6.—Percent differences to the Los Alamos Rosseland mean opacities (LAOL) for the Grevesse (1991) solar composition. The earlier comparisons (*dashed line*) from Iglesias & Rogers (1991b) and the present results (*solid line*) with improved EOS.

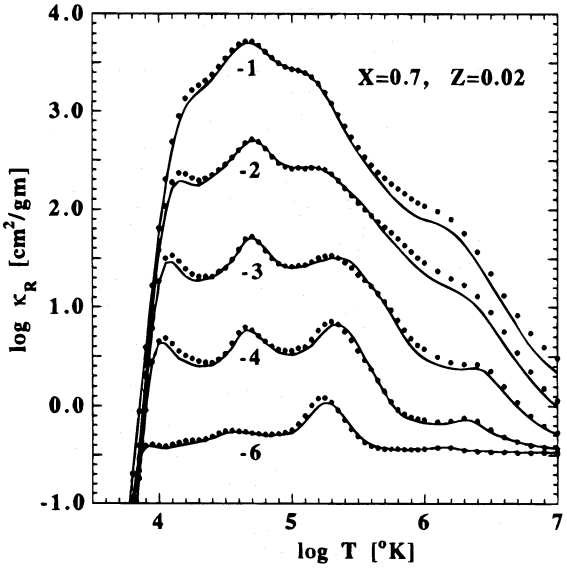

FIG. 7.—Comparison of updated OPAL (*dots*) and OP (*solid line*) Rosseland mean opacities at constant values of log R indicated in the figure where the metal distribution is from SYMP.

sitions in partially filled M-shell Fe ions (Iglesias, Rogers, & Wilson 1987), and later quantified by more complete calculations (e.g., IRW; SYMP) as well as verified by laboratory experiments (Da Silva et al. 1992). Clearly, the opacity in this range of plasma conditions is sensitive to the atomic data (e.g., line energies, oscillator strengths, and line widths), but the details between different calculations are difficult to compare since there are millions of spectral lines contributing to the opacity. It should be noted that both OPAL and OP make approximations in the atomic data generation (see § 7.3 of SYMP for a summary). For example, OPAL uses parametric potentials in the single configuration approximation that neglects "two-electron" jumps and are not as accurate as the close-coupling, multiconfiguration OP calculations. On the other hand, OPAL includes full intermediate coupling where the OP data is computed for pure *LS* in conjunction with a statistical method to account for fine-structure splitting but not intercombination lines. Furthermore, much of the OP results for Fe ions involve the so-called PLUS data (SYMP) and their atomic data for Cr, Mn, and Ni are obtained from extrapolation along iso-electronic sequences of the Fe results. Uncertainties in the line widths can also affect the calculations (Rogers & Iglesias 1992a) and recent measurements (Grenzel & Kunze 1996) show factor of 2 discrepancies between experiments and close-coupling width calculations.

Figures 7 and 8 show significantly larger OPAL opacities for log $R = -1.5$ and log $T > 5.5$ which were noted in the earlier comparisons and were more recently discussed (Iglesias & Rogers 1995) except they now persists to lower R tracks. Recall that in Figure 2*a* there is a considerable opacity increase due to the additional metals (in particular to Ni) at these higher temperatures and log $R = -3.5$. It is then probable that the same source for the discrepancy at log $R = -1.5$ noted in Iglesias & Rogers (1995) applies to Ni at these lower log R tracks.

There remains a discrepancy near log $T = 4.1$ in Figures 7 and 8 that was present in the earlier comparisons (see Fig. 18 of SYMP) but has now increased. At present, the source of this discrepancy has not been identified.

4.3. *Comparison to Alexander & Ferguson*

Comparisons of the updated OPAL opacities to Alexander & Ferguson (1994, hereafter AF94) for a $X = 0.7$ and $Z = 0.02$ composition where the metal distribution is from Grevesse (1991) are given in Figure 9. This figure should be compared to Figure 10 of AF94. It follows that at the lower temperatures the updated OPAL opacities are now in better agreement with AF94. In particular, the updated OPAL results no longer show the oscillations at the lowest temperature. These oscillations in the IRW opacities were due to an error in the table-generation code that combines the individual element monochromatic opacities for a specific composition rather than an error in the photoabsorption calculations.

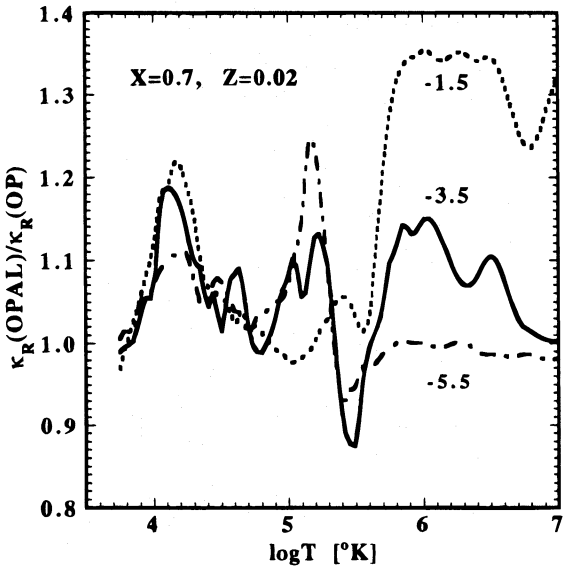

FIG. 8.—Ratio of updated OPAL and OP Rosseland mean opacities for values of log R indicated in the figure for the same composition as in Fig. 7.

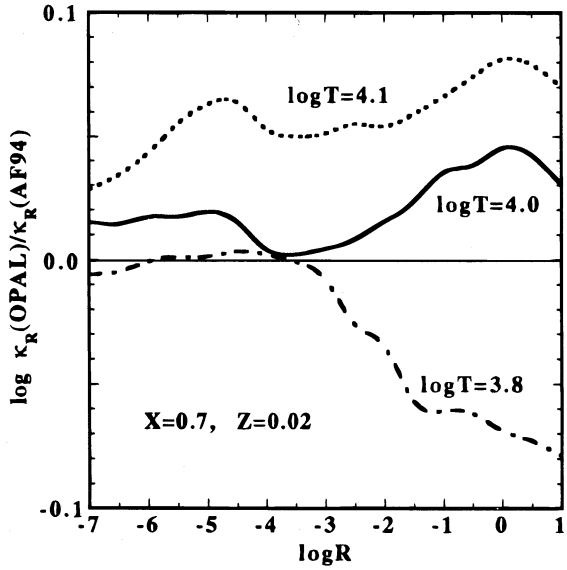

FIG. 9.—Ratio of updated OPAL and AF94 Rosseland mean opacities for $X = 0.7$ and $Z = 0.02$ where the metal distribution is from Grevesse (1991).

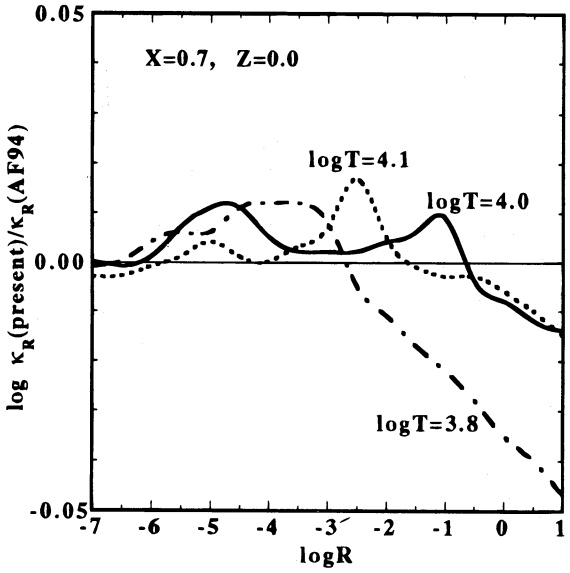

FIG. 10.—Ratio of updated OPAL and AF94 Rosseland mean opacities for $X = 0.7$ and $Z = 0.0$.

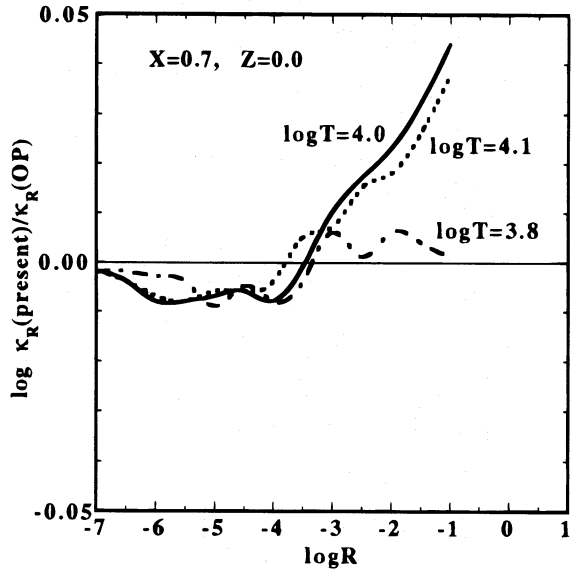

FIG. 12.—Ratio of updated OPAL and OP Rosseland mean opacities for $X = 0.7$ and $Z = 0.0$.

Even though the agreement at log $T = 3.8$ and log $R = +1$ in Figure 9 has improved, which is mostly due to broadening by neutral H and He increasing the opacity by 0.034 dex (see Fig. 3), there remains a 20% (0.079 dex) discrepancy. There are two factors that account for some of the difference at this point: OPAL neglects turbulence in the Doppler broadening and photoabsorption by molecules (except for those in Table 2). These two effects were considered by AF94 and shown to account for 0.008 and 0.014 dex, respectively. These same authors also found that reducing their mixture to the 14 elements in IRW decreased their opacity by 0.022 dex. On the other hand, the change from 14 to 21 elements in the present OPAL calculations only increases the opacity by 0.009 dex. There are elements included by AF94 (all elements up to Cu) still neglected by OPAL, but these neglected elements are considerably lower in abundance. Therefore, it is not expected that including these missing elements would more than double the opacity increase in OPAL already produced by the seven additional metals.

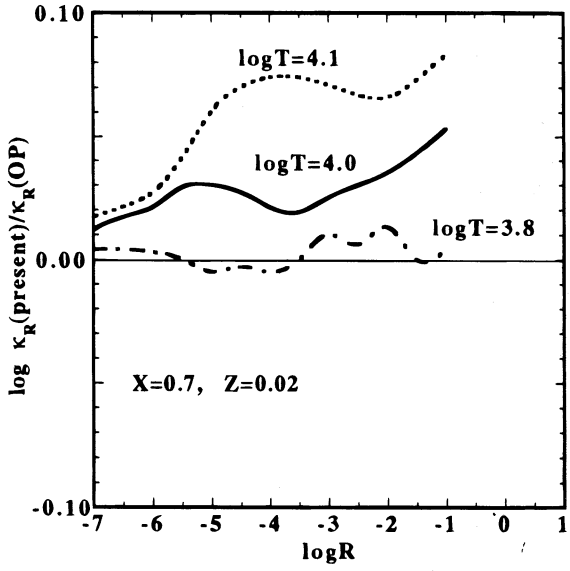

FIG. 11.—Ratio of updated OPAL and OP Rosseland mean opacities for $X = 0.7$ and $Z = 0.02$ where the metal distribution is from SYMP.

An alternative explanation is systematic differences in the two calculations. One possibility is the different treatment of line widths where AF94 uses 3 times the classical damping plus the Unsöld (1955) result while OPAL uses fits to both the impact electron broadening (Rogers & Iglesias 1992a) and broadening by neutral H and He (§ 2.1). A test was performed at log $T = 3.8$ and log $R = +1$ where the line-width fits in OPAL were replaced by the width estimates in AF94. Although the AF94 total line widths are, in general, smaller than those in OPAL, for a portion of the lines most relevant to the opacity the AF94 widths are larger. Thus, the test results yielded a 10% (0.042 dex) opacity increase reducing the discrepancy by about a factor of 2 at these plasma conditions. This opacity increase in OPAL using the AF94 widths combined with the effects of turbulence and molecular absorption reduce the discrepancy to $\sim 3\%$. The improved agreement obtained by the test above, however, only serves to identify a possible source for the discrepancy. That is, any opacity uncertainties due to line broadening have not been reduced, but simply better quantified.

A comparison similar to Figure 11 of AF94 for a zero-metallicity mixture is offered in Figure 10 that shows improved agreement between the two calculations. The discrepancies in Figure 10 are less than 4% except at log $T = 3.8$ and log $R \geq -1$. The latter discrepancies have been slightly reduced by the additional cross sections in Table 2 (see Fig. 4) but remain unexplained. Again, the oscillations at the lowest temperature in the IRW opacities due to a coding error have been removed.

Similar comparisons between OPAL and OP are offered in Figures 11 and 12. Both of these figures show excellent agreement between OPAL and OP at log $T = 3.8$ for log $R \leq -1$ (limit of provided OP data). For the two other temperatures and $Z = 0.02$ the discrepancy is comparable to that in Figure 9. On the other hand, for the zero-metallicity mixture and same 2 temperatures the discrep-

ancy is much larger with OP (but still $\leq 10\%$) than with AF94 at the larger densities. In order to test the sensitivity to line widths, an OPAL calculation using the AF94 width estimates was performed for the $Z = 0.02$ mixture at log $T = 4.1$ and $R = -4.5$, but this only resulted in a 2% (0.009 dex) decrease in opacity. Finally, for the conditions in these figures none of the calculations are in complete agreement, but the largest discrepancies do not exceed 20%.

5. CONCLUSIONS

Updated OPAL opacities have been tabulated for use in stellar models. The modifications include improved physics and numerical procedures as well as corrections. Provided with the opacity tables are codes that allow for interpolation in R, T, X, and Z as well as the C and O mass fractions. These interpolation codes take advantage of the smoothing procedure developed by Seaton (1993) to compute opacity derivatives with respect to temperature and density. Although the distribution of metals in the discussions above emphasized the GN93 solar composition, tables with other metal distributions can be readily computed using a correspondence principle. Request for the tables and supporting codes may be sent to either of the authors or to opal@coral.llnl.gov.

The main change relative to previous OPAL tabulations is a 20% opacity enhancement in the region of the Z-bump for Population I stars. This opacity increase is mostly due to explicitly including more elements in the calculations. A small, but potentially significant, opacity decrease caused by improvements in the equation of state was found for conditions relevant to solar interior conditions. These changes in the OPAL opacities were expected from previous investigations and provided the main motivation for the present revisions.

Comparisons to other recent opacity calculations show reasonably good agreement. In particular, the good agreement with the molecular opacity effort by Alexander & Ferguson (1994) makes it possible to combine the two tabulations smoothly, thus covering the large temperature range generally required in stellar models. There are, however, $\sim 20\%$ discrepancies between the various calculations that remain unexplained.

We gratefully recognize valuable discussions with M. J. Seaton and D. R. Alexander. We also thank D. Saumon for subroutines developed in collaboration with Lenzuni et al. (1991) to compute the collision induced absorption by H_2 and P. T. Springer for bringing the error in the $2s$–$2p$ lines to our attention. With regards to the latter, thanks are due to M. H. Chen for providing accurate atomic data to correct the OPAL parametric potentials. Work performed under the auspices of the Department of Energy by Lawrence Livermore National Laboratory under contract W-7405-Eng-48.

REFERENCES

Adelman, S. J., & Wiese, W. L., ed. 1995, ASP Conf. Ser. 78, Astrophysical Applications of Powerful New Databases (San Francisco: ASP)
Alexander, D. R., & Ferguson, J. W. 1994, ApJ, 437, 879 (AF94)
Bell, K. L. 1980, J. Phys., B13, 1859
Boercker, D. B. 1987, ApJ, 316, L95
Cox, A. N., Morgan, S. M., Rogers, F. J., & Iglesias, C. A. 1992, ApJ, 393, 272
Cox, J. P., & Giuli, R. T. 1968, Principles of Stellar Structure (New York: Gordon and Breech)
Dalgarno, A., & Williams, D. A. 1966, Proc. Phys. Soc. London, 85, 685
Da Silva, L. B., et al. 1992, Phys. Rev. Letters, 69, 438
Deridder, G., & Van Rensbergen, W. 1976, A&AS, 23, 147
Dziembowski, W. A. 1994, in ASP Conf. Ser. 78, Astrophysical Applications of Powerful New Databases, ed. S. J. Adelman & W. L. Wiese (San Francisco: ASP), 275
Dziembowski, W., & Pamyatnykh, A. A. 1993, MNRAS, 262, 204
Elwert, G. 1939, Ann. Phys., 34, 178
Gauschy, A., & Saio, H. 1993, MNRAS, 262, 213
Glenzel, S., & Kunze, H.-J. 1996, Phys. Rev. A, in press
Grevesse, N. 1984, Phys. Sci., T8, 49
———. 1991, A&A, 242, 488(G91)
Grevesse, N., & Noels, A. 1993, in Origin and Evolution of the Elements, ed. N. Pratzo, E. Vangioni-Flam, & M. Casse (Cambridge: Cambridge Univ. Press), 15 (GN93)
Gurtovenko, E. A., & Kondrashova, N. N. 1980, Sol. Phys., 68, 17
Heitler, W. 1954, The Quantum Theory of Radiation, (London: Oxford Univ. Press)
Huang, E. 1987, A&A, 178, 292
Huebner, W. F. 1986, in Physics of the Sun, Vol. I, ed. Sturrock et al. (Dordrecht: Reidel), 33
Huebner, W. F., Merts, A. L., Magee, N. H., & Argo, M. F. 1977, Los Alamos Scientific Report LA-6760-M
Ichimaru, S. 1973, Basic Principles of Plasma Physics (Reading, MA: Benjamin)
Iglesias, C. A., & Rogers, F. J. 1991a, ApJ, 371, L73
———. 1991b, ApJ, 371, 408
———. 1993, ApJ, 412, 752
———. 1995, ApJ, 443, 460
Iglesias, C. A., Rogers, F. J., & Wilson, B. G. 1987, ApJ, 322, L45
———. 1990, ApJ, 360, 221
———. 1992, ApJ, 397, 717 (IRW)
Iglesias, C. A., et al. 1995, ApJ, 445, 855
Itoh, N., Kojo, K., & Masayuki, N. 1990, ApJS, 74, 291
Itoh, N., Masayuki, N., & Kohyama, Y. 1985, ApJ, 294, 17
Kiriakidis, M., El Eid, M. F., & Glatzel, W. 1992, MNRAS, 255, 1P
Koch, H. W., & Motz, J. W. 1959, Rev. Mod. Phys., 31, 920
Lenzuni, P., Chernoff, D. F., & Salpeter, E. E. 1991, ApJS, 76, 759
Luo, G. 1994, A&A, 281, 561
Maxon, S. 1972, Phys. Rev., A5, 1630
Moskalik, P., & Dziembowski, W. 1992, A&A, 256, L5
Rogers, F. J. 1981, Phys. Rev., A24, 1531
Rogers, F. J., & Iglesias, C. A. 1992a, ApJS, 79, 507
———. 1992b, ApJ, 401, 361
———. 1993, in New Prespectives on Stellar Pulsation and Pulsating Variable Stars, ed. J. M. Nemec & J. Mathews (Cambridge: Cambridge Univ. Press), 221
———. 1994, Science, 263, 50
Rogers, F. J., Swenson, F., & Iglesias, C. A. 1996, ApJ, in press
Rogers, F. J., Wilson, B. G., & Iglesias, C. A. 1988, Phys. Rev., A38, 5007
Rozsnyai, B. 1992, ApJ, 393, 409
Sampson, D. H. 1959, ApJ, 129, 734
Seaton, M. J. 1993, MNRAS, 265, L25
Seaton, M. J., Yan, Y., Mihalas, D., & Pradhan, A. K. 1994, MNRAS, 266, 805 (SYMP)
Stancil, P. C. 1994, ApJ, 430, 360
Unsöld, A. 1955, Physics der Sternatmosphären (Berlin: Springer), 269